CRITICAL HEAT FLUX ENHANCEMENT USING HONEYCOMB POROUS PLATE IN A SATURATED POOL BOILING OF WATER-BASED NANOFLUID

Mori S.* and Okuyama K.
*Author for correspondence
Department of Chemical Engineering Science,
Yokohama National University,
Yokohama, Kanagawa 240-8501,
Japan,
E-mail: morisho@ynu.ac.jp

ABSTRACT

A honeycomb-structured ceramic porous plate (HPP) is used for the CHF enhancement in a saturated pool boiling. HPP is commercially available as a filter for purifying exhaust gases from combustion engines. This honeycomb porous plate has considerably smaller micro-pores on the order of 0.1 μm, as compared with those for sintered metal powders, and is simply attached to the test surface without any treatment, such as spraying or sintering. Moreover, the CHF has been enhanced experimentally up to approximately three times that of a plain surface (approximately 320 W/cm^2) with a heated surface of 30 mm in diameter. In this paper, we will show the CHF enhancement mechanism using HPP as well as further CHF enhancement techniques by combination of HPP and nanofluid.

INTRODUCTION

Pool boiling has been used for cooling in numerous thermal energy dissipation systems, such as high-power electronics, heat exchangers, and nuclear reactors. The advantage of pool boiling is that a high heat flux can be removed passively while maintaining a low superheat, as compared with natural/forced convection without phase change. However, the heat removal capacity is limited by the upper limit of cooling, i.e., the critical heat flux (CHF), where the heat transfer coefficient decreases dramatically because the boiling regime is changed from nucleate boiling to film boiling. Therefore, the CHF enhancement is of great interest to engineers and researchers.

Gambill and Lienhard (1989) [1] showed the theoretical upper limit of cooling for evaporation, neglecting condensation on the liquid-vapor interface. The theoretical maximum heat flux is given by

$$q''_{\max} = \rho_v h_{fg} \sqrt{\frac{RT_{sat}}{2\pi M}} \quad (1)$$

where ρ_v, h_{fg}, R, T_{sat}, and M are the density of the vapor, the latent heat of evaporation, the universal gas constant, the saturation temperature, and the molecular mass, respectively. Using Eq. (1), the theoretical maximum heat flux for water is 223.2 MW/m^2 and that for FC-72 is 46.7 MW/m^2 under atmospheric pressure conditions. In general, the achievable CHF for a plain surface without using external power is smaller than the theoretical upper limit for evaporation by one or two orders of magnitude, which indicates that CHF enhancement may be possible.

Except for pool boiling, there are several interesting approaches to extremely high heat flux removal in passive thermal devices (vapor chamber) for electronic cooling [2],[3],[4]. In these studies, water was selected as the test fluid because water has a high surface tension and a large latent heat of vaporization. The reason for the much higher heat flux removal, as compared with the saturated pool boiling CHF for the plain surface (approximately 1 MW/m^2) [5], is that these vapor chambers eliminate the effect of large bubbles formed on the heated surface near CHF conditions in pool boiling. However, the heat-removal performance using these techniques in a vapor chamber depends significantly on the characteristic length of the heated surface because liquid is pumped toward the center of the heated surface by capillary suction [6]. Accordingly, there is advantage to pool boiling in not only removing high heat flux, but also being applicable to large heated surface.

One of the applications for cooling of large heated surface is in-vessel retention (IVR) of corium debris in severe accidents of nuclear power plant [7]. Approaches for increasing the IVR capability must be simple and installable at low cost. In general, the CHF decreases as the heater size increases as stated above [8]. Arik and Bar-Cohen (2003) [8] proposed CHF correlation considering the effect of heater size using the dimensionless heater size, L':

$$L' = \frac{L}{\sqrt{\frac{\sigma}{g(\rho_l - \rho_v)}}} \quad (2)$$

where L is the characteristic heater length. Based on the obtained results, the heat transfer area can be regarded as infinite when L' exceeds approximately 20.

Based on the review of CHF enhancement by surface modification in saturated pool boiling [9-18], CHF is enhanced generally by (1) porous coatings (uniform or modulated) and (2) structures of various sizes fabricated/installed on the heated surface. In general, CHF enhancement in saturated pool boiling is a result of the effects of extended surface area, nucleation site density, wettability, capillary wicking, and wavelength decrease based on the modified Zuber hydrodynamic stability model

[19]. The exact contribution of each effect has not yet been clarified. A number of combined techniques for CHF enhancement have been proposed.

Especially, Mori and Okuyama (2009) [20] proposed novel CHF enhancement technique using a honeycomb-structured ceramic porous plate(see Fig.2), which is commercially available as a filter for purifying exhaust gases from combustion engines, for the CHF enhancement. This honeycomb porous plate (HPP) has considerably smaller micro-pores on the order of 0.1 μm, as compared with those for sintered metal powders, and is simply attached to the test surface without any treatment, such as spraying or sintering. So far the saturated pool boiling CHF (heat source area: ϕ30 mm) is enhanced significantly up to 3.2 MW/m^2 at maximum[21]. To the best of the author's knowledge, the highest value of CHF (3.2 MW/m^2) was obtained for a large heated surface having a diameter of 30 mm.

In this paper, we showed the fundamental effects of HPP on the CHF enhancement, and then further CHF enhancement techniques combing HPP and nanofluid will be shown.

EXPERIMENTAL APPARATUS AND PROCEDURE

EXPERIMENTAL APPARATUS

A schematic diagram of the pool boiling test facility is shown in Fig. 1. The main vessel, which is made of Pyrex glass, has an inner diameter of 87 mm and a height of 500 mm. The pool container was filled with distilled water or nanofluid to a height above the heated surface of approximately 60 mm. The heater component was a copper cylinder having a diameter of 32 mm and a height of 100 mm. The heat flux was supplied to the boiling surface through a copper cylinder using a cartridge electric heater, which was inserted into the copper cylinder and was controlled by an AC voltage regulator. The heat loss from the sides and bottom of the copper cylinder was reduced using a ceramic fiber insulation material.

The top horizontal surface of the copper cylinder, the diameter of which was 30 mm, was smooth and was used as the heat transfer surface in the experiments. The surface is polished using #2000 water-resistant sandpaper before each experiment. Three sheath Type K thermocouples with outer diameters of 1.0 mm were inserted horizontally along the centerline of the copper cylinder. The thermocouples (TC1, TC2, and TC3 in Fig. 1) in the copper cylinder were separated axially by 5.0 mm. The closest thermocouple to the surface was located 10.0 mm below the boiling surface. These thermocouples were calibrated using a platinum resistance thermometer. The measured temperature distribution of TC1 to TC3 was confirmed to be linear. The wall temperature and the wall heat flux were calculated by applying Fourier's Law using TC1 and TC2, where the thermal conductivity of the copper cylinder was evaluated at the arithmetic average temperature of TC1 and TC2.

EXPERIMENTAL PROCEDURE

Experiments were carried out using distilled water or nanofluid as a working fluid under saturated conditions at atmospheric

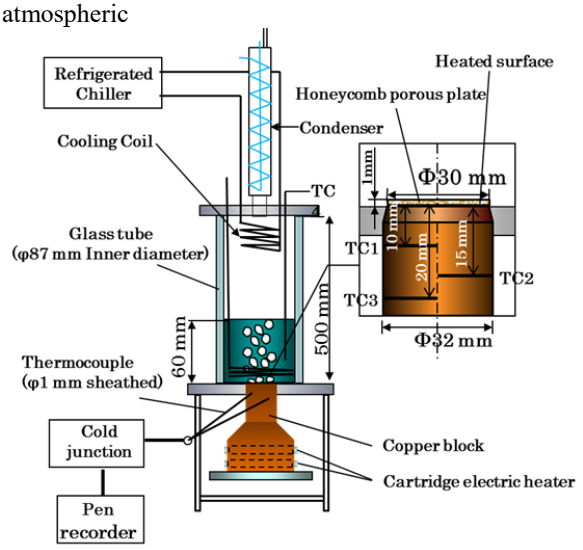

Fig. 1 Schematic diagram of the experimental apparatus.

pressure. A sheathed heater was installed above the heated surface in the liquid bath in order to maintain the liquid temperature at the saturation temperature. For each run, the heat flux was increased in increments of approximately 0.1 MW/m^2 until the CHF condition is reached, which is defined as TC1 rapidly increasing to in excess of 300 °C. All of the measurements were performed in the steady state, which was regarded as being reached when the temperatures did not change more than 0.25 K for at least 10 minutes. When the CHF condition is reached, the heating was immediately stopped in order to prevent damage to the heater or thermocouples. The final heat flux in the quasi-steady state was then measured before the transition to film boiling and was taken as the CHF. All of the measurements were taken only for increasing heat flux, and the effects of hysteresis were not considered.

HONEYCOMB POROUS PLATES

Figure 2 shows the honeycomb porous plate used in the present study. A micrograph of its structure is shown on the right-hand side of the figure. The honeycomb porous plate, which is commercially available, was used as a filter for purifying exhaust gases from combustion engines. The constituent ingredients are $CaOAl_2O_3$ (30-50 wt%), fused SiO_2 (40-60 wt%), and TiO_2 (5-20 wt%). The vapor escape channel width (cell width) d_V, the wall thickness δ_S of the grid, the aperture ratio (ratio of the open area to total area), the height of the honeycomb porous plate δ_h, and the diameter of the honeycomb porous plate are 1.3 mm, 0.4 mm, 0.55, 1.0 mm, and 30.0 mm, respectively. A honeycomb porous plate was attached to the top of the boiling surface by pushing it against the boiling surface using a stainless steel wire (ϕ0.3 mm). The pore radius distribution of the honeycomb porous plates was measured by mercury penetration porosimetry and was found to peak at approximately 0.17 μm. The average pore radius, the

median pore radius, and the porosity of the honeycomb porous plates determined by porosimetry are 0.037 μm, 0.13 μm, and 24.8%, respectively.

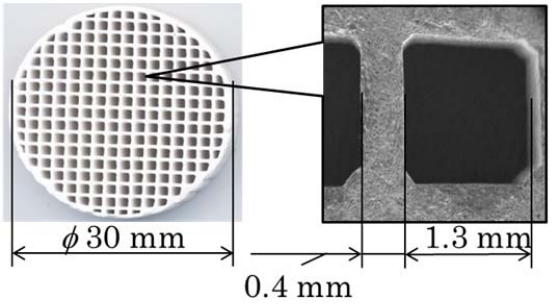

Fig. 2 Honeycomb porous plate.

PREPARATION OF NANOFLUID

The nanoparticle material used in the present study is titanium oxide (TiO_2). The nanosized powders of these materials were purchased from Aerosil Corporation (Aeroxide TiO_2 P 25). The mean size of the dry nanoparticles supplied by the manufacturer was 21 nm. Water-based nanofluids were prepared by dispersing dry powders into distilled water with 2 h of ultrasonic vibration. No additives such as surfactants or dispersants were used to stabilize the nanoparticle suspensions. The concentrations of nanofluid were 0 vol.% (0 g/L), 0.001 vol.% (0.04 g/L), and 0.1 vol.% (4.0 g/L).

UNCERTAINTY ANALYSIS

The individual standard uncertainties are combined to obtain the estimated standard deviation of the results, which is calculated using the law of propagation of uncertainty [31].

The uncertainties of heat flux q, superheat ΔT_{sat}, and heat transfer coefficient h are evaluated using the following equations:

$$\Delta q = \sqrt{\left(\frac{\partial q}{\partial \lambda}\Delta\lambda\right)^2 + \left(\frac{\partial q}{\partial \delta}\Delta\delta_1\right)^2 + \left(\frac{\partial q}{\partial T_1}\Delta T_1\right)^2 + \left(\frac{\partial q}{\partial T_2}\Delta T_2\right)^2} \quad (3)$$

$$\Delta(\Delta T_{sat}) = \sqrt{\left(\frac{\partial(\Delta T_{sat})}{\partial q}\Delta q\right)^2 + \left(\frac{\partial(\Delta T_{sat})}{\partial T_1}\Delta T_1\right)^2 + \left(\frac{\partial(\Delta T_{sat})}{\partial \delta_2}\Delta\delta_2\right)^2 + \left(\frac{\partial(\Delta T_{sat})}{\partial \lambda}\Delta\lambda\right)^2} \quad (4)$$

$$\Delta h = \sqrt{\left(\frac{\partial h}{\partial(\Delta T_{sat})}\Delta(\Delta T_{sat})\right)^2 + \left(\frac{\partial h}{\partial q}\Delta q\right)^2} \quad (5)$$

where T_1 and T_2 are the temperatures at TC1 and TC2, respectively, λ is the thermal conductivity of copper evaluated at the arithmetic mean value of T_1 and T_2, δ_1 is the distance between TC1 and TC2, and δ_2 is the distance between TC1 and the boiling surface. As a result, for the

Relative uncertainties of $\Delta q/q$, $\Delta(\Delta T_{sat})/\Delta T_{sat}$, $\Delta h/h$ and are 2.7 %, 2.7%,and 3.8 % for the case of 1.2 MW/m^2, and 1.8 %, 1.8 %, and 2.5 % for the case of 2.0 MW/m^2, respectively. The relative uncertainties tend to become smaller with increasing heat flux.

EXPERIMENTAL RESULTS AND DISCUSSION

In this section, we will show the fundamental effects of HPP on the CHF enhancement in a saturated boiling of water at first, and then the CHF enhancement combining HPP and nanofluid.

FUNDAMENTAL EFFECTS OF HPP ON THE CHF ENHANCEMENT[20]

EFFECT OF MICRO-PORES AND VAPOR ESCAPE CHANNELS ON THE CHF

Figure 3 shows the boiling curves for different structures of porous plates, i.e., a HPP, a honeycomb solid plate without micro-pores, which was fabricated by impregnating a HPP with adhesive, and a solid porous plate without vapor escape channels, having a height of 5.0 mm. Experiments using a honeycomb solid plate without micro-pores and a solid porous plate without vapor escape channels was carried out in order to clarify the effect of a capillary suction and the effect of vapor channels to avoid an excessive pressure increase in the porous structure on the CHF, respectively. The arrows indicated in Fig. 3 correspond to the CHF condition. As clearly seen from Fig. 3, the CHF for HPP is 1.4 MW/m^2, which is approximately 1.6 times and four times that of the honeycomb solid plate (0.88 MW/m^2) and solid porous plate (0.36 MW/m^2), respectively. These results signify that micro-pores provide strong capillary suction and vapor escape channels are necessary to improve the CHF. That is, the CHF enhancement is attributed to the automatic liquid supply due to capillary action and the reduction of the liquid-vapor counter-flow resistance adjacent to the heated surface due to the separation of the liquid and vapor flow by the honeycomb structure.

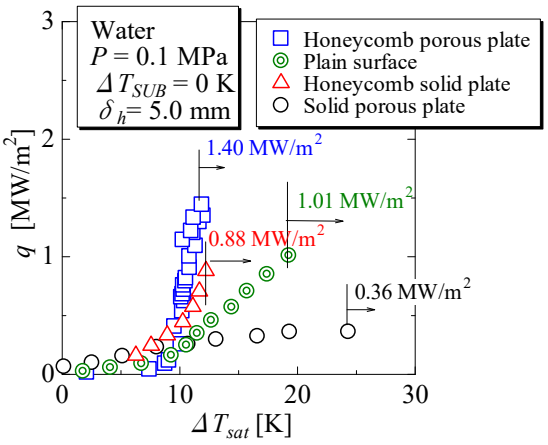

Fig. 3 Boiling curves for different structures of porous plates

EFFECTS OF THE HEIGHTS IN HPPS δ_H ON THE CHF

Figure 4 shows the relationship between the CHF and heights of HPPs. As shown clearly in the figure, the CHF is increased dramatically with the decrease of heights in the HPPs. In particular, a HPP for a height of 1.2 mm can remove the heat flux of 2.5 MW/m^2, which is approximately 2.5 times that of a plain surface (1.0 MW/m^2). The difference in the values of heat-transfer coefficients between different heights (δ_h = 1.2 mm, 5.0 mm, and 10.0 mm) of HPPs are not obvious from boiling curve, although they are significantly large compared with that of a plain surface.

The solid line and the dash-dotted line in this figure indicate the viscous-drag limit predicted by Eq. (8) and the hydrodynamic limit calculated by the model proposed by Liter and Kaviany (2001) [19], respectively. Eq. (8) will be derived in the following section. Comparison of these results will be discussed later. As can be seen in this figure, the CHF increases with the decrease of the height in the HPPs.

The three possible CHF enhancement mechanisms for the use of porous media have been considered. The first is the capillary suction effect. The second is an extended surface area effect, and the third is the effect of a decrease in the flow-critical length scale, or the distance between vapor columns, which is regulated by the modulation in a porous layer, corresponding to Rayleigh-Taylor wavelength in Zuber's hydrodynamic model, as suggested by Liter and Kaviany (2001) [19].

As shown in Fig. 4, the CHF increases significantly as the height of the HPP decreases, which indicates the decrease in the extended surface area. Moreover, considering the low thermal conductivity in the HPPs and the thermal contact resistance between a HPP and a heated surface, the CHF enhancement mechanism in the present phenomena is not related to the extended surface area effect. The hydrodynamic liquid choking limit for the case less than the HPPs height δ_h of approximately 1.2 mm is smaller than the calculated value by the present model as shown in Fig. 4. However, the hydrodynamic limit also may be unrelated to the mechanism in the CHF presented herein even in the case of the HPPs height δ_h of 1.2 mm. As a result, the CHF may be governed by the capillary suction effect. Therefore, it is assumed that the CHF occurs within the porous layer when the viscous drag surpasses the available capillary pumping.

In order to clarify the CHF mechanism, a simplified one-dimensional model, which is similar to the capillary limit model for a conventional heat pipe, applied to the phenomenon, and the calculated results are compared with the observed results.

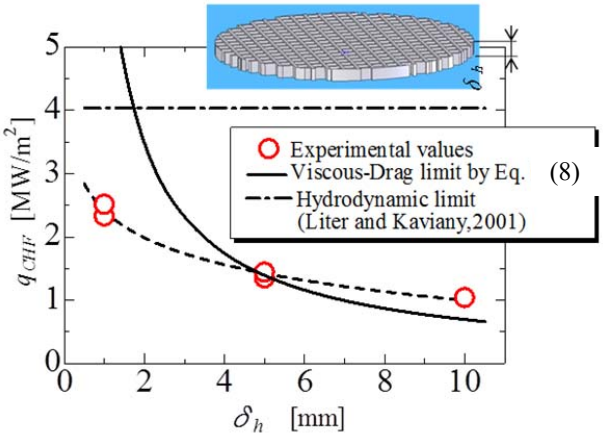

Fig. 4 Relationship between q_{CHF} and height of the honeycomb porous plate

THE CHF MODEL BASED ON CAPILLARY LIMIT

Figure 5 shows a schematic diagram of the steam and water flows in a HPP. As shown in the figure, liquid is transported toward the heated surface within the porous medium by capillary force, and vapor generated in close vicinity to the heated surface escapes upward through the vapor channels. It is assumed that dryout inside the porous material in close to the heated surface does not occur, that is, the inside of the porous material is completely filled with water in order to simplify the model[20].

The CHF is considered to be achieved under conditions such that the maximum capillary pressure $\Delta p_{c,\max}$ is equal to the sum of the pressure losses along the vapor-liquid path in the following:

$$\Delta p_{c,\max} = \Delta p_l + \Delta p_v + \Delta p_a \quad (3)$$

where Δp_l and Δp_v are the frictional pressure drops caused by the liquid flow in the porous medium and the vapor flow through the channels, respectively, and Δp_a is the accelerational pressure drop caused by phase change from liquid to vapor.

The maximum capillary pressure $\Delta p_{c,\max}$ can be calculated by

$$\Delta p_{c,\max} = \frac{2\sigma}{r_{eff}} \quad (4)$$

where r_{eff} is the effective pore radius, and σ is the surface tension.

The pressure drop Δp_l using Darcy's law is expressed as

$$\Delta p_l = \frac{\mu_l Q_{\max} \delta_h}{K A_W \rho_l h_{fg}} \quad (5)$$

where μ_l is the viscosity of the liquid, Q_{max} is the maximum heat transfer rate, δ_h is the height of the HPPs, K is the permeability, ρ_l is the density of a liquid, A_w is the contacted

area of the HPP with the heated surface, and h_{fg} is the latent heat of vaporization.

The vapor pressure drop Δp_v in a laminar incompressible flow (Reynolds number of vapor flow in present work is less than approximately 850) is given by

$$\Delta p_v = \frac{32\mu_v \delta_h Q_{\max}}{\rho_v n d_v^4 h_{fg}} \quad (6)$$

where μ_v is the viscosity of the vapor, and n is the number of the vapor escape channels on the heated surface.

The accelerational pressure drop can be obtained as

$$\Delta p_a = \frac{\rho_v}{2}\left(\frac{Q_{\max}}{(\rho_v n d_v^2) h_{fg}}\right)^2 \quad (7)$$

The following CHF is obtained by substituting Eqs. (4) - (7) into Eq. (3) and using the heated surface area A (approximately 7.07 cm^2), as follows:

$$q_{CHF} = \frac{Q_{\max}}{A} = \frac{-B + \sqrt{B^2 + 4C\left(2\sigma / r_{eff}\right)}}{2AC}, \quad B = \frac{\mu_l \delta_h}{K A_W \rho_l h_{fg}} + \frac{32\mu_v \delta_h}{\rho_v n d_v^4 h_{fg}},$$

$$C = \frac{\rho_v}{2}\left(\frac{1}{(\rho_v n d_v^2) h_{fg}}\right)^2 \quad (8)$$

where the permeability K and the effective pore radius r_{eff} were determined by experimental measurements ($K = 2.4\times10^{-14}\,m^2$, $r_{eff} = 1.6\,\mu m$).

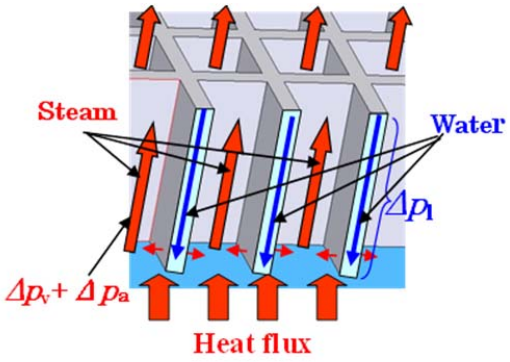

Fig. 5 Schematic diagram of steam and water flows in a honeycomb porous plate

As shown in Fig. 4, both the measured values and the values calculated by Eq. (8) increase as the height of HPP decreases. Moreover, considering the values of the observed CHF are explained roughly by the one-dimensional model, which means two-dimensional effect is not significant on the CHF, the cooling technology using HPPs presented herein may apply to large heated surface area cooling with high heat flux in the saturated pool boiling.

COMBINATION OF HPP AND NANOFLUID[21]

For CHF enhancement in a real IVR application, CHF performance must be considered for conditions such as a HPP in a water with fine particle, rather than pure water, because the HPP may become clogged with particles, resulting in the reduction of CHF. Accordingly, durability tests have been performed for the case of a HPP using nanofluid.

Figure 6 shows the time changes of temperature in TC1 which was installed 10.0 mm below the boiling surface resulting from the addition of nanofluid to pure water in the presence of an attached HPP. The experiment was conducted as follows. First, 900 ml of distilled water was boiled in the presence of an attached HPP. After a steady state was achieved, 100 ml of condensed nanofluid in room temperature was added to boiling pure water so that the final concentration was 0.001 vol.% or 0.1 vol.%. Heat flux is set to approximately 1.8 MW/m^2, which is less than the CHF for the case of an attached HPP in pure water. Interestingly, CHF did not occur under either experimental condition for more than 2 hours. The wall temperature increased suddenly just after the addition of nanofluid because nanoparticles were deposited on the heated surface. The thickness of nanoparticle deposition related to thermal resistance depends on the nanofluid concentration, which is why the temperature increment in thicker nanofluid (0.1 vol.%) is higher than that in thinner nanofluid (0.001 vol.%). The temperature in TC1 then saturates at approximately 100 min in both cases. The amounts of nanoparticles deposited on and detached from the heated surface are considered to be approximately the same. Subsequently, CHF experiments were performed because no burnout is observed under these conditions.

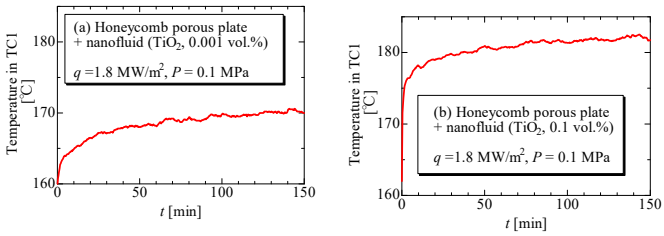

Fig. 6 Time variation of TC1 just after the addition of nanofluid to pure water (final nanofluid concentration: (a) 0.001 vol.%, (b) 0.1 vol.%).

Figure 7 shows the relationship between the CHF and concentration of nanofluid. As shown in this figure, for the case of a nanofluid only, the CHF increases up to 1.7 MW/m^2 (pure water: 1.0 MW/m^2), and the CHF is not affected by the nanofluid concentration. On the other hand, the CHF is increased up to more than 2 MW/m^2 by attaching a HPP to the heated surface in pure water as reported in a previous study[20]. The CHF with a HPP increases as the nanofluid concentration increases, and, surprisingly, the CHF reaches approximately 3.2 MW/m^2 at maximum for 0.1 vol.% nanofluid. The CHF was increased significantly, by approximately three times that for the case of pure water on a plain surface.

Detailed SEM observations were carried out in order to clarify the behavior at the clearance between the HPP and the heated surface.

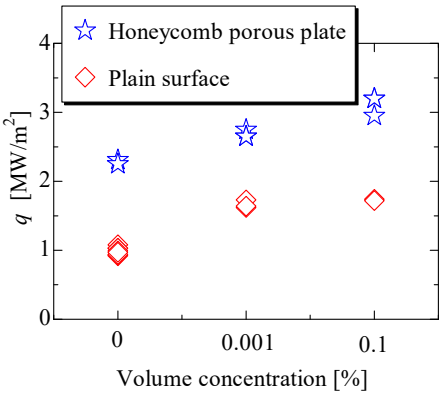

Fig. 7 Schematic drawing of Two-layer structured honeycomb porous plate

Figure 8 shows SEM images below the surface of the HPP attached to the heated surface (a) before and (b) after the CHF experiments for 0.1 vol.% nanofluid. As shown in the figures, nanoparticles were deposited beneath the HPP after the experiment. Moreover, micro-channels of several tens of microns in width were formed just below the HPP. Microchannels formed near the heated surface may decrease the flow resistance for escaping vapor in the porous layer due to nanoparticle deposition, resulting in increased CHF enhancement.

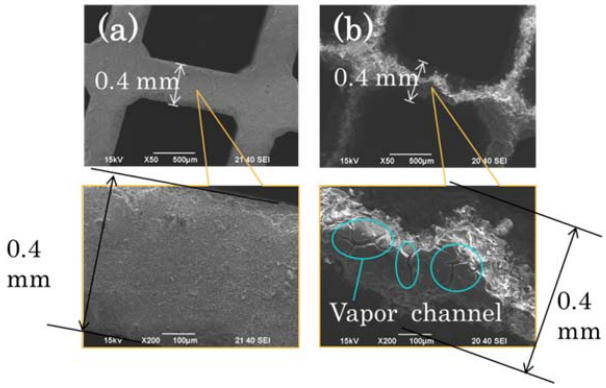

Fig. 8 SEM images of the bottom surface of a honeycomb porous plate (a) before the boiling experiment and (b) after the boiling experiment (nanofluid: 0.1 vol.%).

Based on the above discussion, the CHF enhancement mechanism resulting from the combination of a HPP and a nanofluid is considered as follows. A nanoparticle deposition layer is formed on the heated surface. The surface wettability and capillary wicking performance are improved due to the nanoparticle-deposited surface. Therefore, dryout is retarded due to nanoparticle deposition once a liquid is supplied by gravity to the heated surface through vapor escape channels from the top surface, in addition to this effect, liquid is supplied to heated surface due to capillary action by the HPP as shown previous studies [20, 22], resulting in CHF enhancement significantly.

As a result of the attachment of a HPP to a heated surface in a nanofluid, CHF enhancement in saturated pool boiling occurs due to the effects of wettability, capillary wicking, the inflow of liquid through vapor escape channels, and vapor escaping macro- and micro-channels. The exact contribution of each effect has not yet been clarified.

CONCLUSION

CHF enhancement in saturated pool boiling is a result of the effects of extended surface area, nucleation site density, wettability, capillary wicking, and change of hydrodynamic wavelength. The exact contribution of each effect has not yet been clarified. In this paper, CHF enhancement technique using HPP in a saturated pool boiling was introduced. A honeycomb-structured porous plate is commercially available as a filter for purifying exhaust gases from combustion engines, and this method can be applicable to high heat flux removal (up to approximately 3.2 MW/m^2 combining the HPP and nanofluid) of large heated surface.

ACKNOWLEDGEMENTS

This study includes the result of “Establishment of In- Vessel Retention using novel passive cooling technology” carried out under the Initiatives for Atomic Energy Basic and Generic Strategic Research by the Ministry of Education, Culture, Sports, Science and Technology of Japan.

REFERENCES

[1] W. Gambill, J. Lienhard, An upper bound for the critical boiling heat flux, Journal of Heat Transfer, 111(3) (1989) 815-818.
[2] T. Semenic, I. Catton, Experimental study of biporous wicks for high heat flux applications, International Journal of Heat and Mass Transfer, 52(21-22) (2009) 5113-5121.
[3] M. Hashimoto, H. Kasai, K. Usami, H. Ryoson, K. Yazawa, J.A. Weibel, S.V. Garimella, Nano-structured two-phase heat spreader for cooling ultra-high heat flux sources, in: the 14th International Heat Transfer Conference, Washington, DC, USA, 2010.
[4] J. Weibel, S. Kim, T.S. Fisher, S.V. Garimella, Carbon nanotube coatings for enhanced capillary-fed boiling from porous microstructures, Nanoscale and Microscale Thermophysical Engineering, 16(1) (2012) 1-17.
[5] N. Zuber, Hydrodynamic aspects of boiling heat transfer AECU-4439, Phisics and Mathematics, US Atomic Energy Commission, (1959).
[6] T. Semenic, High Heat Flux Removal Using Biporous Heat Pipe Evaporators, University of California, Los Angeles, 2007.
[7] J.L. Rempe, K.Y. Suh, F.B. Cheung, S.B. Kim, In-Vessel

Retention of molten corium: lessons learned and outstanding issues, Nuclear Technology, 161 (2007) 210 - 267.
[8] M. Arik, A. Bar-Cohen, Effusivity-based correlation of surface property effects in pool boiling CHF of dielectric liquids, International Journal of Heat and Mass Transfer, 46(20) (2003) 3755-3764.
[9] H.S. Ahn, M.H. Kim, A review on critical heat flux enhancement with nanofluids and surface modification, Journal of Heat Transfer, 134(2) (2012) 024001.
[10] J.N. Chung, T. Chen, S.C. Maroo, A Review of Recent Progress on Nano/Micro Scale Nucleate Boiling Fundamentals, Frontiers in Heat and Mass Transfer, 2(2) (2011) 1-19.
[11] R. Kamatchi, S. Venkatachalapathy, Parametric study of pool boiling heat transfer with nanofluids for the enhancement of critical heat flux: A review, International Journal of Thermal Sciences, 87 (2015) 228-240.
[12] H. Kim, Enhancement of critical heat flux in nucleate boiling of nanofluids: a state-of-art review, Nanoscale research letters, 6(1) (2011) 415.
[13] Y.W. Lu, S.G. Kandlikar, Nanoscale Surface Modification Techniques for Pool Boiling EnhancementA Critical Review and Future Directions, Heat Transfer Engineering, 32(10) (2011) 827-842.
[14] S.M.S. Murshed, C.A. Nieto de Castro, M.J.V. Lourenço, M.L.M. Lopes, F.J.V. Santos, A review of boiling and convective heat transfer with nanofluids, Renewable and Sustainable Energy Reviews, 15(5) (2011) 2342-2354.
[15] C.M. Patil, S.G. Kandlikar, Review of the Manufacturing Techniques for Porous Surfaces Used in Enhanced Pool Boiling, Heat Transfer Engineering, 35(10) (2014) 887-902.
[16] X.-Q. Wang, A.S. Mujumdar, Heat transfer characteristics of nanofluids: a review, International Journal of Thermal Sciences, 46(1) (2007) 1-19.
[17] R.L. Webb, The Evolution of Enhanced Surface Geometries for Nucleate Boiling, Heat Transfer Engineering, 2(3-4) (2007) 46-69.
[18] J.M. Wu, J. Zhao, A review of nanofluid heat transfer and critical heat flux enhancement—Research gap to engineering application, Progress in Nuclear Energy, 66 (2013) 13-24.
[19] S.G. Liter, M. Kaviany, Pool-boiling CHF enhancement by modulated porous-layer coating: theory and experiment, International Journal of Heat and Mass Transfer, 44(22) (2001) 4287-4311.
[20] S. Mori, K. Okuyama, Enhancement of the critical heat flux in saturated pool boiling using honeycomb porous media, International Journal of Multiphase Flow, 35(10) (2009) 946-951.
[21] S. Mori, S. Mt Aznam, R. Yanagisawa, K. Okuyama, CHF enhancement by honeycomb porous plate in saturated pool boiling of nanofluid, Journal of Nuclear Science and Technology, (2015) 1-8.
[22] S. Mori, S. Mt Aznam, K. Okuyama, Enhancement of the critical heat flux in saturated pool boiling of water by nanoparticle-coating and a honeycomb porous plate, International Journal of Heat and Mass Transfer, 80 (2015) 1-6.